









pubs.acs.org/joc

A Theoretical Stereoselectivity Model of Photochemical Denitrogenations of Diazoalkanes Toward Strained 1,3-**Dihalogenated Bicyclobutanes**

Jingbai Li, Rachel Stein, and Steven A. Lopez*



Cite This: J. Org. Chem. 2021, 86, 4061-4070



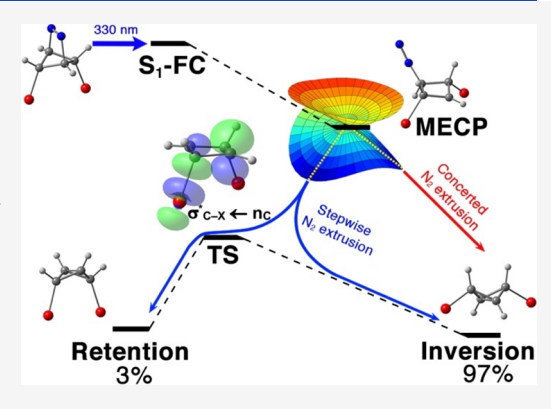
ACCESS I

III Metrics & More

Article Recommendations

s Supporting Information

ABSTRACT: Photochemical reactions exemplify "green" chemistry and are an essential tool for synthesizing highly strained molecules under mild conditions with light. The light-promoted denitrogenation of bicyclic azoalkanes affords functionalized, stereoenriched bicyclo [1.1.0] butanes. These reactions were revisited with multireference calculations and non-adiabatic molecular dynamics (NAMD) simulations to provide a detailed analysis of the photophysics, reactivities, and unexplained stereoselectivity of a series of diazabicyclo [2.1.1] hexenes. We used complete active space self-consistent field (CASSCF) calculations with an (8,8) active space and ANO-S-VDZP basis set; the CASSCF energies were corrected with CASPT2 (8,8)/ANO-S-VDZP. The nature of the electronic excitation is $n \to \pi^*$ and ranges from 3.77 to 3.91 eV for the diazabicyclo [2.1.1] hexenes reported here. Minimum energy path calculations showed stepwise C-N bond breaking and led directly to a minimum energy crossing point, corresponding to a stereochemical "double



inversion" product. Wigner sampling of diazabicyclo[2.1.1]hexene provided initial conditions for 692 NAMD trajectories. We identified competing complete stereoselective and stereochemical scrambling pathways. The stereoselective pathways feature concerted bicyclobutane inversion and N2 extrusion. The stereochemical scrambling pathways involve N2 extrusion followed by bicyclobutane planarization, leading to stereochemical scrambling. The predicted diastereomeric excess (d.e.) almost exactly matches the experiment (calc.d.e. = 46% vs exp.d.e. = 47%). Our NAMD simulations with 672, 568, and 596 trajectories for 1-F, 1-Cl, and 1-Br predicted a d.e. of 94-97% for the double inversion products. Halogenation significantly perturbs the potential energy surface (PES) toward the retention products due to hyperconjugative interactions. The $n_C \to \sigma^*_{C-X, X=F, Cl, Br}$ hyperconjugative effect leads to a broader shoulder region on the PES for double inversion.

■ INTRODUCTION

Photochemical transformations offer efficient access to highly strained molecular architectures under mild reaction conditions and a light source. Photochemistry falls under the umbrella of green chemistry because it does not require rareearth organometallic catalysts or extended periods of reaction heating to achieve the same reaction outcome. The lightpromoted denitrogenation is one of the cleanest and most convenient reactions because the byproduct is nitrogen gas. One important and underexplored reaction is the denitrogenation of cyclic azoalkanes, for instance diazabicyclo [2.1.1] hex-2-ene (1) to afford bicyclo [1.1.0] butane (2) under thermal conditions.1

Bicyclo[1.1.0]butane is the most strained carbon-based bicycle with the strain energy approaching 66 kcal mol⁻¹.2 The central σ_{C-C} bond bends the plane of two cyclopropane exposing the p-orbitals that can function as nucleophiles^{3,4} or electrophiles.4. These properties make bicyclo[1.1.0]butanes a privledged class of molecules with broad applications. 5-7 The synthesis and functionalization of bicyclo[1.1.0]butane is

challenging because of the high strain energy and propensity to engage in side reactions. The current functionalization can only access bridgehead carbons, implying that the chemical potential of bicyclo[1.1.0] butane has not been fully exploited. Scheme 1 summarizes synthetic routines to prepare bicyclo[1.1.0]butane and the derivatives.^{8–12}

The decomposition of cyclic azoalkanes toward carbonbased bicycles has been extensively studied by thermolysis^{8,13-15} and photolysis¹⁶ in solution,⁸ gas phase,¹³ or solidstate.¹⁷ Dougherty and co-workers have investigated the deuterated diazabicyclo[2.1.1]hex-2-ene (1-D). They measured a 47% excess of exo-2-D in the singlet-state photolysis 16 (Scheme 2), while the thermolysis of 1-D afforded stereo-

Received: December 8, 2020 Published: February 5, 2021





Scheme 1. Synthesis of Bicyclo[1.1.0]Butane

Scheme 2. Diastereoselectivity in the Direct Photolysis of Cyclic Azoalkanes

random products likely due to symmetric cyclobutane diradical intermediates.¹³ Later, Roth and co-workers have discovered a diastereoselective denitrogenation mechanism of irradiating diazabicyclo [2.2.1]hept-2-ene (3) and discovered a 20% diastereomeric excess of the inverted product *exo-4-2D*¹⁸ (Scheme 2). Trofimov and co-workers studied the temperature and solvent effect on the stereoselectivity^{19,20} and confirmed a general preference for inversion across several derivatives of 3.²¹ Adam and co-workers performed a photochemical reaction involving a benzene photosensitizer, but observed no diastereomeric excess as forming the cyclopentane diradical intermediate.²²

Quantum mechanical calculations have provided detailed insights into the photochemical stereoselectivities of 1 and 3. In 1998, Olivucci and Robb located and characterized a diazenyl diradical conical intersection of 3 with a complete active space self-consistent field (10 electron and 8 orbitals) and 6-31G* basis set, which suggested a preferred inversion mechanism.²³ In 2003, Olivucci and co-workers published a single classical trajectory with the B3LYP/6-31G* model chemistry to understand the reaction path from their previously located diazenyl diradical conical intersection. They concluded that the stereoselectivity was attributed to an impulsively populated inversion vibrational mode.²⁴ Li and co-workers then located a diazenyl diradical conical intersection of 1 with a 12 electron and 10 orbitals active space and 6-311G** basis set in 2006; the minimum energy path proceeded to the double-inversion product.²⁵ Most recently, Abe and co-workers reviewed that the interplay between diazenyl and 1,3-diyl diradicals is responsible for the stereoselectivity during the denitrogenation of cyclic azoalkanes.²⁶ These theoretical reports offer qualitative rationale for the stereoselectivity; we identified an opportunity to quantify the origin of the measured diastereomeric excess.

We revisited photophysics and photochemistry of 1 with multiconfigurational calculations and used non-adiabatic molecular dynamics simulations to quantify the stereoselectivity. The dynamics simulations uncovered the mechanistic origin of the stereoselectivity in the denitrogenation of 1. We applied our dynamics model to predict the stereoselectivities of a series of 1,3-dihalogenated diazabicyclo[2.1.1]hexa-2-enes, as shown in Scheme 3 (1-F,

Scheme 3. 1,3-Dihalogenated Diazabicyclo[2.1.1]hexa-2-ene and Proposed Denitrogenation

1-Cl, and 1-Br). In particular, we are interested in 1,3-dibromo diazabicyclo[2.1.1]hexa-2-ene (1-Br) because it enables the access to the cyclic carbon in the bicyclo[1.1.0]butane derivative (2-Br) for subsequent fluorination, chlorination, and alkylation reactions toward value-added molecules and materials. Our computations will show the halogenation effect on the stereoselectivities in the denitrogenation.

We identified four reaction coordinates (R1, R2, a, and θ) to track the geometries of 1 and 1-Br, along the ground- and excited-states. R1 represents the length of the first breaking C-N bond and R2 is the length of the second breaking C-N bond. We defined an angle θ to determine the bicyclobutane dihedral between the cyclopropyl rings. We introduced the hydrogen dihedral angle a to describe the relative position of the hydrogen atom on the bond-breaking carbon atom with respect to the cyclopropyl plane. Figure 1 shows the distance R1 and R2 and dihedral angle θ and a in S₀-1-Br and MECP-1-Br.

Potential Energy Surface Scans. We computed potential energy surfaces (PESs) for 1, 1-F, 1-Cl, and 1-Br with complete active space self-consistent field (CASSCF) (8,8)/ANO-S-VDZP by scanning the bicyclobutane dihedral angle, θ from 160 to 200° and the hydrogen dihedral angle a from -20 to 20° with a 4° step size for θ and a. We constrained one of the C–N bonds to 1.48 Å to prevent the dissociation of N₂ in 1-F, 1-Cl, and 1-Br, which often led to unconverged geometries. The PESs of 1 are nearly identical with and without the C–N bond constraint. We also computed PESs for 2, 2-F, 2-Cl, and 2-Br with CASSCF (2,2)/ANO-S-VDZP by

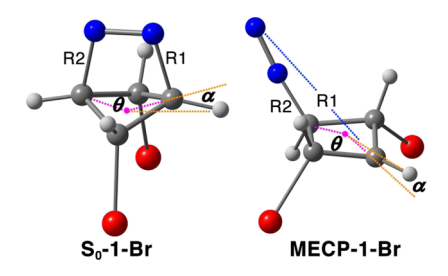


Figure 1. CASSCF (8,8)/ANO-S-VDZP optimized geometries of $\mathbf{S_0}$ –**1-Br** and **MECP-1-Br**. The pink dotted lines highlight the bicyclobutane dihedral angle θ between the cyclopropyl rings. The θ values <0 (i.e., -180 to 0°) were converted to a range, $180-360^\circ$. The yellow dotted lines show the hydrogen dihedral angle a between the cyclopropyl plane and the hydrogen atom sharing the same edge of θ . a > 0, when the hydrogen atom is above the cyclopropyl plane; a < 0, when the hydrogen atom is under the cyclopropyl plane. The blue dotted line indicated the R1 distance in the broken C-N bond. In $\mathbf{S_0}$ –**1-Br**, R1 = R2 = 1.56 Å, θ = 136°, and a = -17° ; in **MECP-1-Br**, R1 = 4.35 Å, R2 = 1.41 Å, θ = 197°, and a = 5° . The optimized geometries for 1, 1-F, and 1-Cl are available in the Supporting Information.

removing nitrogen atoms and corresponding active orbitals. The scan of the hydrogen dihedral angle *a* constrained both bridge-head hydrogen atoms and varied them simultaneously.

Non-adiabatic Molecular Dynamics. Non-adiabatic molecular dynamics (NAMD) simulation classically propagates the nuclear positions on potential energy surfaces obtained from multiconfigurational electronic calculation. We sampled the initial conditions (nuclear positions and velocities) from the vibrational modes in Wigner distribution at 300 K. The electronic calculations used CASSCF (8,8)/ANO-S-VDZP. The trajectories started from the S₁ Franck-Condon point and the simulation time was 300 fs with a 0.5 fs time step. We applied the Nosé-Hoover thermostat³⁵ to equilibrate the ensemble temperature at 300 K. The surface hopping probability was computed with Tully's fewest switches surface hopping method^{36–38} implemented in OpenMolcas.²⁷

Natural Bond Orbital Analysis. We quantified the carbon-halogen bond hyperconjugations in the transition state between the retention and inversion products using the natural bond orbital (NBO) analysis³⁹ implemented in GenNBO6.0.40 The orbital interactions were computed using second order perturbation of the Fock matrix in NBO basis (i.e., E(2) energy).³⁹ The E(2) energy is defined as E(2) = $F_{\rm d,a}^2/\Delta E_{\rm d,a}$, where $F_{\rm d,a}$ is the one-electron integral over donor and acceptor orbitals and $\Delta E_{\rm d,a}$ is the orbital energy difference. The E(2) energy is positive, which indicates the magnitude of the energetic stabilization gained from orbital interactions. The single point calculations employed PBE041,42 density functional and cc-pVDZ⁴³ basis set available in ORCA 4.2.0.⁴⁴ We used the broken-symmetry formalism⁴⁵ of density functional theory to properly address the multiconfigurational characters in the transition state structures.

■ RESULTS AND DISCUSSION

Photoexcitation of 1 and 1-Br. The electronic excitation of 1 is a well-known $n \to \pi^*$ transition; this corresponds to an excitation of an electron from a diazo nitrogen lone pair orbital (n) to its $\pi^*_{N=N}$ -orbital. We have computed the photophysical properties to validate the (8,8) active space for 1 and its halogenated derivatives. Table 1 shows the computed

S₁ excitation energies, electronic transitions, and oscillator strengths.

Table 1. Vertical Excitation Energies, Electronic Transitions, and Oscillator Strengths of 1 and 1-X (X = F, Cl, and Br) with CASPT2 (8,8)/ANO-S-VDZP//CASSCF (8,8)/ANO-S-VDZP

compounds	S ₁ energy (eV)	transition	oscillator strength ^a
1	3.91	$n\rightarrow\pi^*$	$1.13 \cdot 10^{-2}$
1-F	3.79	$n \rightarrow \pi^*$	$8.53 \cdot 10^{-3}$
1-Cl	3.78	$n \rightarrow \pi^*$	$6.80 \cdot 10^{-3}$
1-Br	3.77	$n\rightarrow\pi^*$	$6.26 \cdot 10^{-3}$

^aOscillator strengths are computed with CASSCF (8,8)/ANO-S-VDZP.

The CASPT2 (8,8)/ANO-S-VDZP//CASSCF (8,8)/ANO-S-VDZP calculation of 1 predicted an S_1 state with $n\pi^*$ character. The excitation energy was 3.91 eV, which agrees with the experimental absorbance $\lambda_{\text{max}} = 330 \text{ nm} (3.75 \text{ eV}).^8$ The oscillator strength for this transition is $1.13 \cdot 10^{-2}$. The halogenated reactants (1-F, 1-Cl, and 1-Br) have lower excitation energies (3.77-3.79 eV, respectively) and lower oscillator strengths (8.53-6.26·10⁻³). The decreasing oscillator strength suggests that the halogen atoms may result in a lower quantum yield for these reactants due to less efficient $n\rightarrow\pi^*$ excitations. Our CASSCF (8,8)/ANO-S-VDZP calculations overestimated the excitation energies because of the missing electronic dynamic correlations (Table S1). The CASSCF (8,8)/ANO-S-VDZP calculations predicted a consistent $n \rightarrow \pi^*$ transition and thus is qualitatively reliable to study the photochemistry of 1 and 1-Br from the S₁ Franck-

We computed the minimum energy path (MEP) to explore the steepest descent path from S_1 -FC-1 and S_1 -FC-1-Br. The MEP from S_1 -FC-1 has been previously reported by Li and coworkers. Our new calculations on 1-F and 1-Cl showed similar MEP to the parent 1 (Figure S3), while 1-Br offers a substantially different MEP starting from S_1 -FC-1-Br (Figure 2).

The MEP in Figure 2 shows that the mechanism involves a stepwise breaking of the C-N bonds. The MEP suggests that there may be an S_1 barrier (steps 1-4), this "local maximum" may be an artifact resulting from the CASPT2 (8,8)/ANO-S-VDZP single point energy calculations. The CASSCF (8,8)/ ANO-S-VDZP MEP decreased smoothly (Figure S4). The ΔS_1 and S₀ states decreases along the MEP and is <0.50 eV at step 10, where one of the C-N bonds has completely broken (R1 = 3.62 Å). Beyond this point, the MEP energies are nearly constant until the S₁/S₀ degeneracy region. We optimized a minimum energy crossing point based on the geometry at step 24 and located MECP-1-Br. The geometry of MECP-1-Br clearly shows inversion; the θ angle is 197° (Figure 1). From MECP-1-Br, the MEP calculation proceeded along the S₀ state. The subsequent path showed the second C-N bond breaking. Step 28 shows that the N-C distance R2 was 2.10 Å, while the bicyclobutane maintained an inverted dihedral angle of 216°. We located exo-2-Br and an extruded N2 at the end of the MEP. Our MEP calculations have developed a static understanding of the photochemistry of 1-Br and suggest that exo-2-Br is exclusively formed through a stepwise pathway.

Non-adiabatic Molecular Dynamics of 1. Experimental measurements of the photochemical reaction yield of

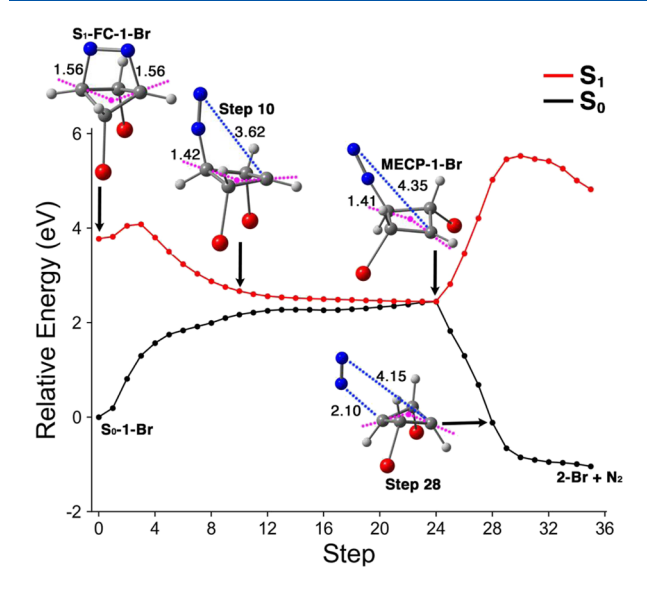


Figure 2. Minimum energy path from S₁-FC-1-Br to MECP-1-Br and to 2-Br with CASPT2 (8,8)/ANO-S-VDZP//CASSCF (8,8)/ANO-S-VDZP. The blue dotted lines denote the C–N distance; the distances are in Angstrom. The pink dotted lines highlight the bicyclobutane dihedral angle θ . At step 10, R1 = 3.62 Å, R2 = 1.42 Å, θ = 159°, and a = -9°; at step 28, R1 = 4.15 Å, R2 = 2.10 Å, θ = 216°, and a = -20°.

diazabicyclo[2.1.1]hexenes (1) reveals an excess yield of bicyclo[1.1.0]butane with inverted stereochemistry. We turned to NAMD simulations to enumerate the possible photodynamics pathways and predict the yield of the competing stereoisomeric products. We have generated initial conditions for 1 with Wigner sampling at 300 K to create a broad region of Franck-Condon points and associated velocities. The initial geometries have sampled the C–N distances to range from 1.33 to 1.68 Å, the bicyclobutane dihedral angle θ = 115–138°, and the hydrogen dihedral angle $a = - (8-32)^\circ$. Our NAMD results for 1 are based on 692 trajectories for which 395 (57%) trajectories land on the ground-state with stepwise breaking of

the C-N bonds, consistent with the static MEP findings. The other 297 (43%) trajectories remain in the S₁ state at the end of 300 fs; we consider these trajectories to correspond to unfinished reactions. We identify three pathways post S_1/S_1 intersections: the reversal to reactant 1, the double-inversion product exo-2, and the retention product endo-2. Our simulations show a major product, exo-2 (71%), minor products, endo-2 (26%), and the reactant, 1 (3%). The predicted diastereomeric excesses of exo-2 (46%) is in excellent agreement with the experiments (47% 16). Emboldened by this excellent agreement with the experiment, we sought to understand the bonding changes along the groundand excited-state reaction pathways to reveal the origin of the stereoselectivity of 1. We first plotted the trace of productive trajectories with respect to the distance of the first breaking C-N bond, R1, and the bicyclobutane dihedral angle as shown in Figure 3a. The subplots in Figure 3b-e highlight individual types of pathways during the second N-C bond breaking.

The molecular trajectories rapidly moved away from the FCregion and approach hopping points (Figure 3a). The trajectories switched the electronic state to the ground-state via surface hopping points near/at the S₁/S₀ degeneracy region; 8% of the trajectories had "early" hopping points with a single partially broken N-C bond has not been fully broken $(R1 = 1.49 - 2.16 \text{ Å and } \theta = 125 - 139^{\circ})$. We identified a broad S_1/S_0 seam in the other trajectories (R1 = 2.95–4.77 Å and θ = 142-235°) (Figure 3a). We found that 60% trajectories retained the bicyclobutane dihedral angle (θ < 180°) at the S₁/ S_0 seam. However, tracking the dihedral angle, θ showed subsequent conversion from endo-2 to exo-2 in 42% trajectories. On the other hand, 32% trajectories have shown double inversion ($\theta > 180^{\circ}$) at the S_1/S_0 seam, but 6% of the trajectories reverted from exo-2 to endo-2 towards the end of the simulations. The interconversion between exo-2 and endo-2 trajectories after the surface hopping points suggests that the S₁/S₀ intersection partially control the stereoselectivity and ground-state effects may also be important.

After the S_1/S_0 crossing, the trajectories of 1 (Figure 3b and Figure 4e) show that the second C-N bond continues to

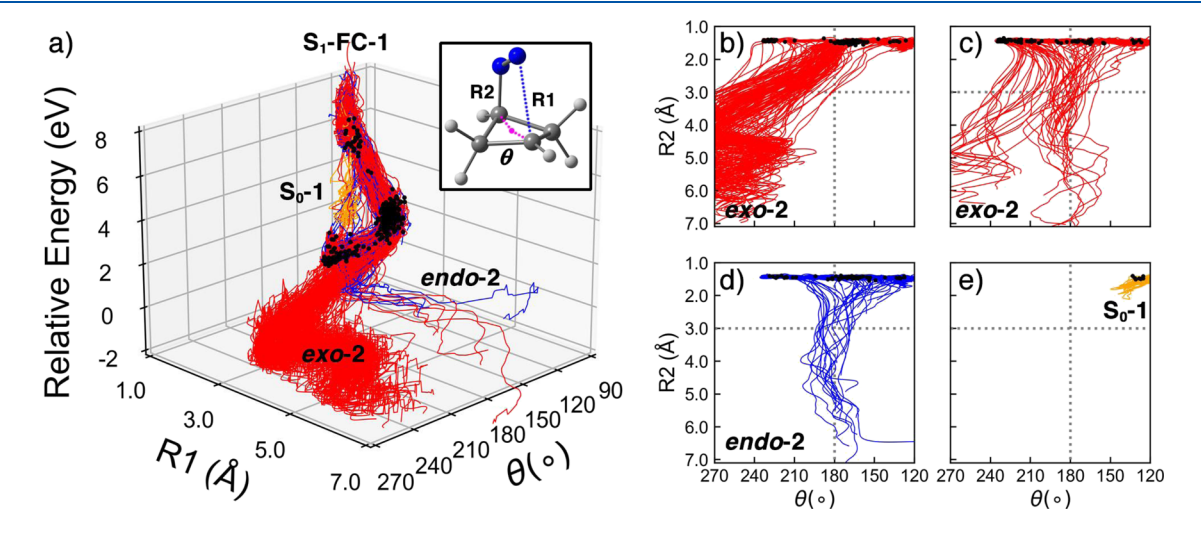


Figure 3. (a) Trajectories of 1 in 300 fs NAMD simulation with CASSCF (8,8)/ANO-S-VDZP. The plot monitors the N–C bond breaking and bicyclobutane inversion with R1 and θ . (b) Subplot of trajectories undergoing concerted N–C bond breaking and bicyclobutane inversion to exo-2. (c) Subplot of trajectories undergoing stepwise N–C bond breaking and bicyclobutane inversion to exo-2. (d) Subplot of trajectories undergoing stepwise N–C bond breaking and bicyclobutane retention to endo-2. (e) Subplot of trajectories reverted to S_0 -1. The subplots (b–e) track the second C–N bond breaking and the inversion of bicyclobutane with R2 and θ . The black dots represent the latest surface hopping points.

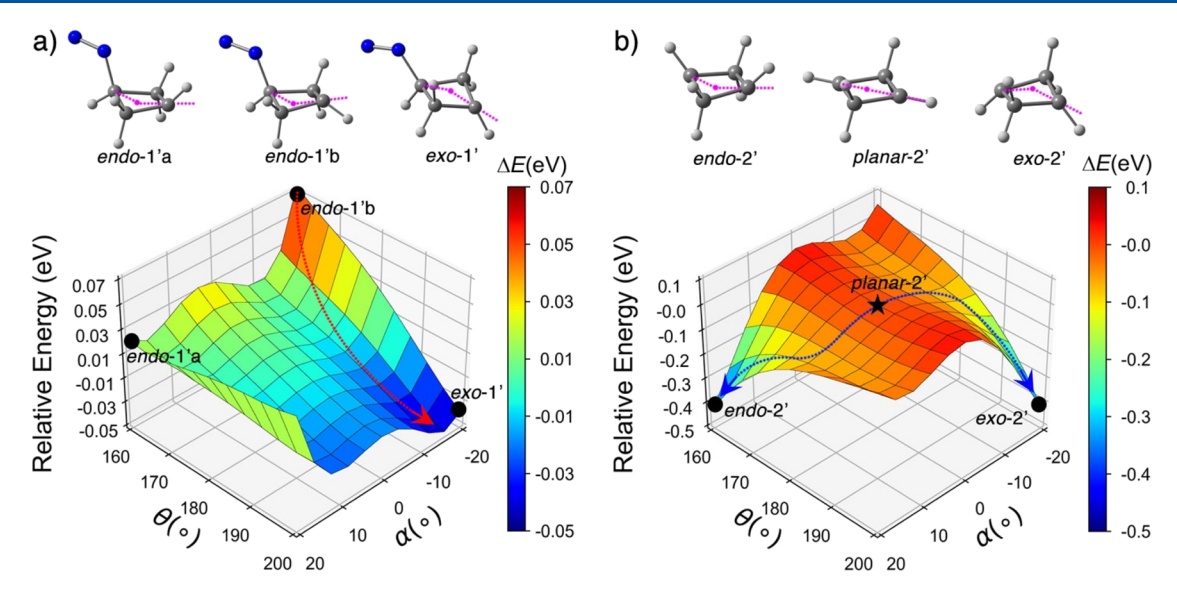


Figure 4. (a) 2D PES of **1** with CASSCF (8,8)/ANO-S-VDZP. The red dotted arrow shows the deepest descent toward inverted bicyclobutane. (b) 2D PES of **2** with CASSCF (2,2)/ANO-S-VDZP. The blue dotted arrows represent the symmetrically bifurcated relaxation paths to the retention and inversion structure. The star in (b) is a second-order saddle point with CASSCF (2,2)/ANO-S-VDZP. The first imaginary mode corresponds to concerted vibrating of *a*, whereas the second imaginary mode represents stepwise alternating of *a*, which cannot be seen in (b). The geometries at black dots (star) are shown above the 2D PES.

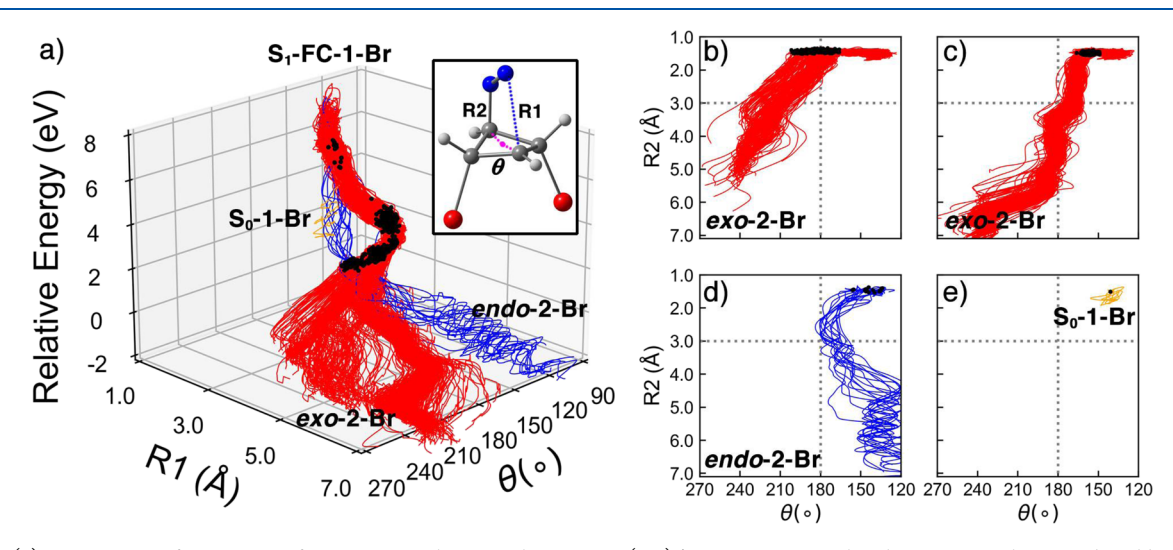


Figure 5. (a) Trajectories of 1-Br in 300 fs NAMD simulation with CASSCF (8,8)/ANO-S-VDZP. The plot monitors the N–C bond breaking and bicyclobutane inversion with R1 and θ . (b) Subplot of trajectories undergoing concerted N–C bond breaking and bicyclobutane inversion to *exo*-2-Br. (c) Subplot of trajectories undergoing stepwise N–C bond breaking and bicyclobutane inversion to *exo*-2-Br. (d) Subplot of trajectories undergoing stepwise N–C bond breaking and bicyclobutane retention to *endo*-2-Br. (e) Subplot of trajectories reverted to 1-Br. The subplots (b–e) track the second C–N bond breaking and the inversion of bicyclobutane with R2 and θ .

lengthen. We classified two ground-state mechanisms in these trajectories: (1) the second N–C bond breaking and the bicyclobutane inversion are occurring simultaneously (concerted mechanism) and (2) the second C–N bond breaking and the bicyclobutane inversion are occurring in a stepwise manner. All of the trajectories corresponding to the concerted mechanism are stereoselective to form *exo-2* (48% trajectories, Figure 3b). The stepwise mechanism extrudes N₂ before inverting (i.e., θ). The resulting bicyclobutane molecule with θ > 210° then retained the dihedral angle θ , which favors *exo-2* (Figure 3c). The trajectories with θ < 210° vibrate about θ = 180° (Figure 3c,d). The stepwise mechanism results in an overall ratio of 0.9: 1 between *exo-2* and *endo-2* (23 and 26% of the productive trajectories, respectively). Figure 3e characterizes the trajectories returned to 1. It showed that

these trajectories were from the early S_1/S_0 crossing region; they revert to 1 because the C-N bonds are partially broken.

The trajectories show that the denitrogenation reaction begins in the S_1 state and completes on the S_0 -state through a concerted or stepwise mechanistic pathway. To understand the ground-state topology of 1 and the stereoselectivity of the reaction, we computed the 2D PES of the ground states of 1. Figure 4a,b shows the 2D PES scanned with the bicyclobutane dihedral angle θ and the hydrogen dihedral angle a of 1.

Figure 4a is a ground-state PES for the concerted mechanism and the black dots correspond to the hopping points based on the trajectories in Figure 3b ($\theta = 126-234^{\circ}$ and $a = -32-24^{\circ}$). There is a steep pathway (indicated with a red arrow) from $\theta = 160$ to 180° and from $a = -20^{\circ}$ to -16° that is consistent with preferred conversion of *endo-2* to *exo-2*

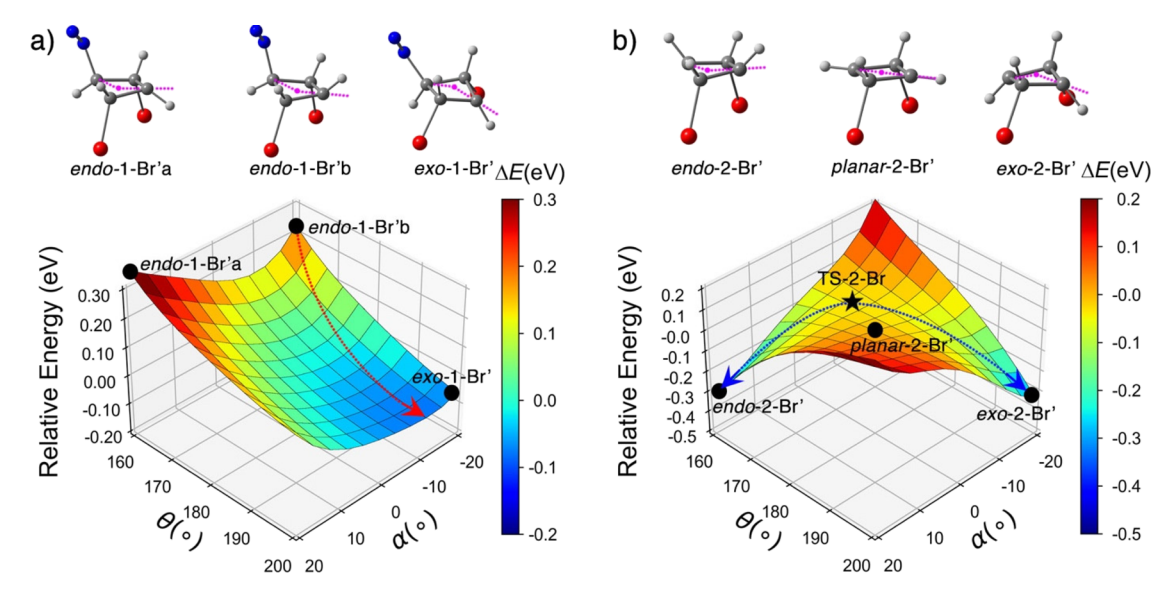


Figure 6. (a) 2D PES of **1-Br** with CASSCF (8,8)/ANO-S-VDZP, where the N–C distance was constrained at 1.48 Å. The red dotted arrow shows a path favoring the inversion of bicyclobutane. (b) 2D PES of **2-Br** with CASSCF (2,2)/ANO-S-VDZP. The blue dotted arrows represent the asymmetrically bifurcated relaxation paths, which is more inclined toward the inversion structure. The star in (b) was confirmed as a transition state with CASSCF (2,2)/ANO-S-VDZP. The geometries at black dots are shown above the 2D PES.

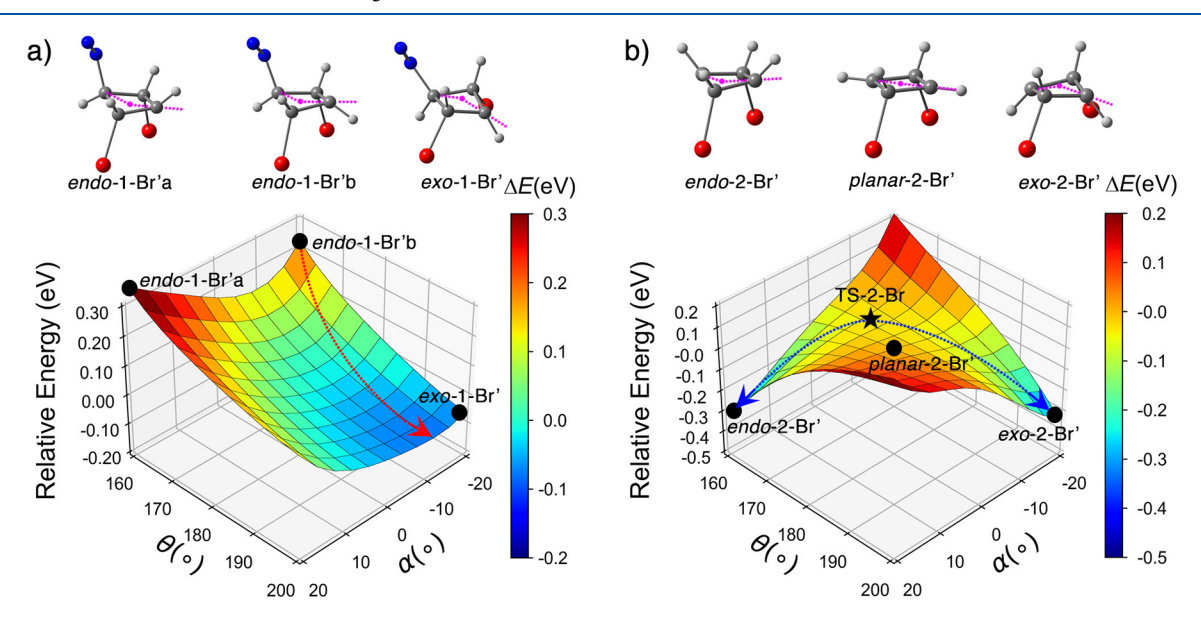


Figure 7. (a) Optimized geometry of TS-2-Br with CASSCF (2,2)/ANO-S-VDZP. $\theta = 171^{\circ}$ and $a = -6^{\circ}$. (b) Hyperconjugation of $n_C \to \sigma^*_{C-Br}$ in terms of natural bond orbital interactions in TS-2-Br (left) and the planar 2-Br (right). The E (2) energies are in kcal mol⁻¹.

in the NAMD results discussed above. It also corroborates the previous interpretation of the stereoselectivity induced by impulsive population of the double-inversion vibrations. We note that R1 in *exo-1'* (4.39 Å) is longer than that in *endo-1b'* (4.15 Å). It suggests the *exo* geometry stabilizes the diradical configuration with further separated radical centers. As shown in Figure 4b, N_2 is omitted and the ground-state PES of 2 is used to approximate the PES for the stepwise mechanism. We assume that the trajectories start near the center of the 2D PES ($\theta = 180^{\circ}$ and $a = 0^{\circ}$) because most of the trajectories vibrate around $\theta = 180^{\circ}$ as shown in Figure 3c,d. The relaxation pathways bifurcate toward the local minima at $\theta = 160^{\circ}$; $a = 20^{\circ}$ and $\theta = 200^{\circ}$; $a = -20^{\circ}$, which resemble *endo-2* and *exo-2*, respectively. The symmetric pathways are consistent with the nearly equal *endo-2* and *exo-2* product ratio.

Non-adiabatic Molecular Dynamics of 1-Br. We extended our analysis of the reactivity, mechanism, and stereoselectivity beyond 1 to explore the excited-state landscape of halogenated diazabicyclo [2.1.1] hexenes (1-Br). We chose 1-Br because it is the experimental precursor to 1-F and 1-Cl, which can be accessed with a thermal substitution reaction. As such, we performed NAMD simulations of 1-Br to study substitution effects on the stereochemical outcomes when irradiating 1 and 2. We extended our previous computational technique to these reactants; 525 trajectories of 1-Br landed on the ground-state (out of 596) after 1 ps, indicating a reaction "yield" of 88%. This is considerably larger than that of the parent 1. The increasing photolysis efficiency of 1-Br could compensate for the weakened absorption ability predicted by the oscillator strengths (Table 1). Our trajectory statistics demonstrate that 97% trajectories formed exo-2-Br, whereas 3% formed *endo-2-Br*, which corresponds to a predicted diastereomeric excess of 94% for *exo-2-Br*. We also observed a single trajectory that reverts to S_0-1 -Br (0.2%). The trajectories from S_1 -FC-1-Br are plotted with respect to distance of the first breaking C–N bond, R1, and the bicyclobutane dihedral angle as shown in Figure 5a. The subplots in Figure 5b–d highlight the concerted, stepwise, and reverted mechanism during the second C–N bond breaking of 1-Br.

The denitrogenation of 1-Br—like the parent—begins in the excited-state and completes in the ground state. The trajectories reached exo-2-Br via a S_1/S_0 crossing seam at R1 = 3.50-4.63 Å and $\theta = 149-202^{\circ}$. At the S_1/S_0 seam, 28% trajectories inverted the bicyclobutane (θ >180°) and maintained the angle in exo-2-Br. 71% trajectories retain the bicyclobutane dihedral angle θ (θ <180°), but only 2% trajectories conserved θ to form *endo-2-Br* when they hopped to the ground-state. Another 1% of the trajectories passed a S_1 / S_0 crossing region at R1 = 1.67-2.35 Å and θ = 134-148° toward endo-2-Br. Figure 5b shows the concerted second C-N bond breaking and bicyclobutane inversion toward exo-2-Br (43% trajectories). Figure 5c,d shows the stepwise mechanism where N₂ is extruded before the bicyclobutane inverts. In contrast to the nearly 1:1 ratio in the parent, the 1-Br trajectories undergoing stepwise mechanism significantly prefer exo-2-Br (54% trajectories) over endo-2-Br (3% trajectories). Figure 5e illustrates the single trajectory that reverts to S_0-1 -

We again computed the 2D PESs of 1-Br to understand the topologies and rationalize the mechanism and predicted stereoselectivity of 1-Br. The PESs scanned along the bicyclobutane dihedral angle θ and the hydrogen dihedral angle a are shown in Figure 6a and Figure 7b.

The 2D PES scan of 1-Br in Figure 6a surveys the concerted mechanism; the second C-N bond is constrained at 1.48 Å to prevent N₂ from extruding at some geometries. We marked the hopping points in Figure 6a that correspond to the S_1/S_0 seam geometries (θ =149–202°, Figure 5a). The PES shows a local minimum at $\theta = 200^{\circ}$ and $a = -12^{\circ}$ that resembles an inverted bicyclobutane. This suggests that 1-Br is stereoselective for exo-2-Br with the concerted mechanism, which is consistent with the stereoselectivity of the parent. Figure 6b shows the PES for the stepwise mechanism, where the N₂ has already dissociated. The PES of 1-Br is quite different from the corresponding PES shown in Figure 4b. The PES for 1-Br is not symmetric like that of 1; the transition structure connecting exo-2 and endo-2 is in the center of the PES. The transition structure connecting exo-2-Br and endo-2-Br (TS-2-Br) is skewed toward the disfavored product, endo-2-Br. We hypothesized that the unsymmetric PES disproportionately lowered the energies of exo-like geometries. It arose from a hyperconjugative interaction between the carbon lone pair orbital and the $\sigma^*_{\mathrm{C-Br}}$ -orbital. For example, the C–Br distance in TS-2-Br is 2.00 Å, which is 0.08 Å longer than the that in 1-Br (1.92 Å). This increase in the $\sigma_{\text{C-Br}}$ bond length and the antiperiplanar relationship between the lone pair (n_C) and the σ^*_{C-Br} orbitals suggests that a favorable $n_C \rightarrow \sigma^*_{C-Br}$ hyperconjugation occurs. Figure 7 illustrates the NBOs participating in TS-2-Br and planar-2-Br' along with their second-order perturbation interaction energy, E(2).

At the PES center in Figure 6b, *planar-2-Br'* is 0.7 kcal mol⁻¹ higher than that in TS-2-Br (Figure 6b). The *E* (2) of TS-2-Br is 0.6 kcal mol⁻¹ larger than that of *planar-2-Br'*,

which suggests the bicyclobutane dihedral angle θ = 171° can lower the transition state energy with $n_C \to \sigma^*_{C-Br}$ hyperconjugative interactions. Consequently, the transition structure changes its relative position from the center of the PES (*planar-2-Br'*) toward *endo-2-Br* thus resulting in larger shoulder region for relaxation to *exo-2-Br*. Based on Figure 5c,d, we can assume the trajectories post S_1/S_0 surface hopping start at θ = 160–200°; thus, most of them (54% νs 3%) land on the ground-state path toward *exo-2-Br*.

Our collaborators in the Burns group (Stanford University) are actively verifying our computational results with photolysis experiments of 1-Br. The preliminary and unpublished results suggest the predicted denitrogenation mechanism of 1-Br might be the first step in a series of complex photoreaction of 1-Br.

Non-adiabatic Molecular Dynamics of 1-F and 1-Cl. We extended our computations to include two theoretical diazabicyclo[2.1.1]hexenes, 1-F and 1-Cl. We performed 672 and 568 NAMD trajectories to test our hypotheses. The simulations predicted 87% "yield" in 1-F and 1-Cl, which are similar to 1-Br (88%). The major products of 1-F and 1-Cl preferred double inversion (exo-2-F: 98% vs endo-2-F: 1% and exo-2-Cl: 98% vs endo-2-Cl: 2%). Our trajectories predicted a diastereomeric excess of 97 and 96%, respectively. The trajectory characterization (Figures S5 and S6) confirmed the coexistence of concerted and stepwise N₂ extrusion mechanisms in 1-F and 1-Cl. The PES calculations for fluorinated and chlorinated derivatives (Figures S7 and S8) illustrated that the concerted mechanism also favors double inversion. In the stepwise mechanism, we observe a similar broad path to the corresponding inverted products, thus enhancing the stereoselectivities. We located transition structures analogous to TS-2-Br, TS-2-F, and TS-2-Cl, which show a similar structural pyramidalization [TS-2-F: $\theta = 174^{\circ}$; TS-2-Cl: $\theta = 169^{\circ}$]. We interpret this as a necessary structural change to benefit from the $n_C \rightarrow \sigma^*_{C-F,Cl}$ hyperconjugative interaction (Figure S9). Therefore, the post surface hopping trajectories of 1-F and 1-Cl with $\theta = 180 \pm 10^{\circ}$ favor the steeper path to double

CONCLUDING REMARKS

Our NAMD simulation shows a consistent halogenation effect that substantially enhances the stereoselectivity in the photochemical denitrogenation of 1 producing nearly exclusive double inversion products. We have used CASSCF calculations with an (8,8) active space and ANO-S-VDZP basis set to study the photophysics and photochemistries of 1, 1-F, 1-Cl, and 1-Br. Our calculations and NAMD simulations predict that photochemistry of 1-F, 1-Cl, and 1-Br will be efficient and favor double inversion pathways and products.

The CASPT2 (8,8)/ANO-S-VDZP//CASSCF (8,8)/ANO-S-VDZP calculations presented here suggest that 1, 1-F, 1-Cl, and 1-Br will feature $n \to \pi^*$ transitions with excitation energies ranging from 3.77 to 3.91 eV. The minimum energy path calculation of 1-Br showed stepwise C-N bond breaking and characterized a minimum energy crossing point that favors double inversion. We computed 692 NAMD trajectories of 1 and identified competing stereoselective and nonstereoselective paths; 48% trajectories followed the stereoselective paths, where the N_2 extrusion and bicyclobutane inversion were occurring simultaneously. The nonstereoselective paths extruded N_2 with a nearly planar bicyclobutane; 23 and 26% of the trajectories led to *exo-2* and *endo-2*, respectively. The total

trajectories undergoing the two mechanisms successfully reproduced the stereoselective double inversion of **2** (calc.*d.e.* = 46% vs exp.*d.e.* = 47%).

Our calculations suggest that halogenation of leads to stereoselective in the photochemical denitrogenation reactions of 1. We predict a considerably higher stereoselectivity of double inversion than 1 with 94% diastereomeric excess of exo-2-Br. The increase stereoselectivity results from the stepwise N₂ extrusion mechanism in which 54% trajectories favored the exo-2-Br and 3% trajectories lead to endo-2-Br. The static PES calculations showed that TS-2-Br was skewed toward endo-2-Br resulting in a broader relaxation path to exo-2-Br. Consequently, most of post-surface-hopping trajectories in the stepwise mechanism with nearly planar geometries in 2-Br $(\theta = 180 \pm 10^{\circ})$ favor the pathway to exo-2-Br. Our calculations reveal is TS-2-Br 0.7 kcal mol⁻¹ lower in energy than that planar-2-Br' because of stabilizing the hyperconjugative $(n_C \rightarrow \sigma^*_{C-Br})$ interactions. We find similar results in 1-F and 1-Cl, which demonstrate the essential role of $n_C \rightarrow \sigma^*_{C-X, X} = F, Cl. Br$ hyperconjugation on the increased stereoselectivity for halogenated diazabicyclo[2.1.1]hexenes.

COMPUTATIONAL METHODS

Multiconfigurational Calculations. Our multiconfigurational calculations employed the state-averaged CASSCF with single-state CASPT2 corrections, implemented in OpenMolcas 19. 11.27 In the previous study on the unsubstituted 1 and 3, Li²⁵ and Olivucci²⁴ have constructed an active space consisting of 12 electrons and 10 orbitals (i.e., (12,10)), featuring four electrons from the $\sigma_{N=N}/\sigma^*_{N=N}$ and $\pi_{N=N}/\pi^*_{N=N}$ orbitals, four electrons from two lone pair orbitals $(n_{N=N})$ of endocyclic nitrogens, and four electrons from two sets of $\sigma_{\rm C-N}$ σ^*_{C-N} orbitals. We chose an active space of eight electrons and eight orbitals because the nitrogen lone pair orbitals become less active during state averaging in the reactant with the occupations near 2.00. In the (8,8) active space, the second σ_{C-N} orbital is notably localized on nitrogen atoms showing nonbonding character, consistent with a previous time-dependent density functional theory study by Ciofini and co-workers.²⁸ The (8,8) space reproduced the excitation energy corresponding to the experimental absorption spectrum. The (8,8) active space requires substantially reduced computational cost relative to the (12,10) space. As such, we chose it for our state-averaged CASSCF calculations. Figure 8 illustrates the orbitals and average occupancies of our selected (8,8) active space in 1-Br.

The optimized geometries with the (8,8) space used the ANO-S-VDZP basis set.^{29–32} Subsequent vibrational analysis confirmed that

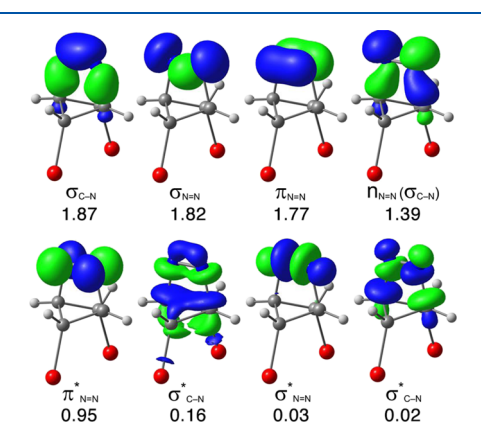


Figure 8. (8,8) active space of **1-Br**. The occupation numbers are averaged over seven states, computed at CASSCF (8,8)/ANO-S-VDZP. Isosurface value = 0.08. The active spaces for **1**, **1-F**, and **1-Cl** are available in the Supporting Information.

ground-state geometry, S_0 –1, S_0 –1-F, S_0 –1-Cl, and S_0 –1-Br, were indeed local minima with all positive frequencies. We performed MEP calculations from the S_1 -Franck-Condon point. We optimized S_1/S_0 minimum energy crossing points (MECP-1, MECP-1-F, MECP-1-Cl, and MECP-1-Br) with CASSCF (8,8)/ANO-S-VDZP. The CASPT2 (8,8) corrections to the electronic energy included a shift of 0.3 Hartree to avoid intruder states. 33,34

ASSOCIATED CONTENT

Supporting Information

The Supporting Information is available free of charge at https://pubs.acs.org/doi/10.1021/acs.joc.0c02905.

Active spaces, optimized geometries, CASSCF excitation energies, CASSCF minimum energy paths for 1, 1-F, 1-Cl, and 1-Br, NAMD trajectories for 1-F and 1-Cl, 2D PES for 1-F, 2-F, 1-Cl, and 2-Cl, hyperconjugation in 2-F and 2-Cl, and Cartesian coordinates for optimized geometries (PDF)

AUTHOR INFORMATION

Corresponding Author

Steven A. Lopez — Department of Chemistry & Chemical Biology, Northeastern University, Boston, Massachusetts 02115, United States; orcid.org/0000-0002-8418-3638; Email: s.lopez@northeastern.edu

Authors

Jingbai Li — Department of Chemistry & Chemical Biology, Northeastern University, Boston, Massachusetts 02115, United States

Rachel Stein – Department of Chemistry & Chemical Biology, Northeastern University, Boston, Massachusetts 02115, United States

Complete contact information is available at: https://pubs.acs.org/10.1021/acs.joc.0c02905

Notes

The authors declare no competing financial interest.

ACKNOWLEDGMENTS

J.L. and S.A.L. acknowledge Dr. Jordan M. Cox for helpful discussion on the NAMD trajectories. S.A.L. acknowledges the Office of Naval Research (ONR N00014-12-1-0828) and the National Science Foundation (NSF-1940307) for funding this research. R.S. acknowledges funding from the National Science Foundation (NSF DBI-2031778). J.L., R.S. and S.A.L. appreciate the assistance from the Northeastern Research Computing Team and access to the computing resources of the Discovery cluster.

REFERENCES

- (1) Horváth, I. T.; Anastas, P. T. Innovations and green chemistry. *Chem. Rev.* **2007**, *107*, 2169–2173.
- (2) Khoury, P. R.; Goddard, J. D.; Tam, W. Ring strain energies: substituted rings, norbornanes, norbornenes and norbornadienes. *Tetrahedron* **2004**, *60*, 8103–8112.
- (3) Fawcett, A.; Biberger, T.; Aggarwal, V. K. Carbopalladation of C-C sigma-bonds enabled by strained boronate complexes. *Nat. Chem.* **2019**, *11*, 117–122.
- (4) Gianatassio, R.; Lopchuk, J. M.; Wang, J.; Pan, C. M.; Malins, L. R.; Prieto, L.; Brandt, T. A.; Collins, M. R.; Gallego, G. M.; Sach, N. W.; Spangler, J. E.; Zhu, H.; Zhu, J.; Baran, P. S. Organic chemistry. Strain-release amination. *Science* **2016**, *351*, 241–246.

- (5) Chen, K.; Huang, X.; Kan, S. B. J.; Zhang, R. K.; Arnold, F. H. Enzymatic construction of highly strained carbocycles. *Science* **2018**, 360, 71–75.
- (6) Fawcett, A. Recent advances in the chemistry of bicyclo- and 1-azabicyclo [1.1.0] butanes. *Pure Appl. Chem.* **2020**, 92, 751–765.
- (7) Walczak, M. A.; Krainz, T.; Wipf, P. Ring-strain-enabled reaction discovery: new heterocycles from bicyclo[1.1.0]butanes. *Acc. Chem. Res.* **2015**, *48*, 1149–1158.
- (8) Chang, M. H.; Dougherty, D. A. 2,3-Diazabicyclo [2.1.1] hex-2-ene. Synthesis and thermal decomposition. *J. Org. Chem.* 1981, 46, 4092–4093.
- (9) Gaoni, Y. Preparation of ring-substituted (arylsulfonyl)-cyclopropanes and (arylsulfonyl)bicyclobutanes from .gamma.,.del-ta.-epoxy sulfones. *J. Org. Chem.* **1982**, *47*, 2564–2571.
- (10) Panish, R.; Chintala, S. R.; Boruta, D. T.; Fang, Y.; Taylor, M. T.; Fox, J. M. Enantioselective synthesis of cyclobutanes via sequential Rh-catalyzed bicyclobutanation/Cu-catalyzed homoconjugate addition. J. Am. Chem. Soc. 2013, 135, 9283–9286.
- (11) Tokunaga, K.; Sato, M.; Kuwata, K.; Miura, C.; Fuchida, H.; Matsunaga, N.; Koyanagi, S.; Ohdo, S.; Shindo, N.; Ojida, A. Bicyclobutane Carboxylic Amide as a Cysteine-Directed Strained Electrophile for Selective Targeting of Proteins. *J. Am. Chem. Soc.* **2020**, *142*, 18522–18531.
- (12) Wipf, P.; Stephenson, C. R.; Okumura, K. Transition-metal-mediated cascade reactions: C,C-dicyclopropylmethylamines by way of double C,C-sigma-bond insertion into bicyclobutanes. *J. Am. Chem. Soc.* **2003**, *125*, 14694–14695.
- (13) Chang, M. H.; Dougherty, D. A. Phase-dependent stereochemistry and chemical activation in the thermal decomposition of 2,3-diazabicyclo[2.1.1]hexene. *J. Am. Chem. Soc.* **1982**, *104*, 1131–1132.
- (14) Chang, M. H.; Jain, R.; Dougherty, D. A. Chemical activation as a probe of reaction mechanism. Synthesis and thermal decomposition of 2,3-diazabicyclo[2.1.1]hex-2-enes. *J. Am. Chem. Soc.* **1984**, *106*, 4211–4217.
- (15) Peterson, T. H.; Carpenter, B. K. Estimation of dynamic effects on product ratios by vectorial decomposition of a reaction coordinate. Application to thermal nitrogen loss from bicyclic azo compounds. *J. Am. Chem. Soc.* **1992**, *114*, 766–767.
- (16) Chang, M. H.; Dougherty, D. A. Photochemistry of 2,3-diazabicyclo[2.1.1]hex-2-ene. .beta. Carbon-carbon cleavage to a stereorandom triplet biradical. *J. Am. Chem. Soc.* **1982**, *104*, 2333–2334.
- (17) Adam, W.; García, H.; Martí, V.; Moorthy, J. N.; Peters, K.; Peters, E.-M. Photochemical Denitrogenation of Norbornene-Annelated 2,3-Diazabicyclo[2.1.1]hept-2-ene-Type Azoalkanes: Crystal-Lattice versus Zeolite-Interior Effects. *J. Am. Chem. Soc.* **2000**, *122*, 3536–3537.
- (18) Roth, W. R.; Martin, M. Zur Stereochemie des thermischen und photochemischen Zerfalls von 2.3-Diaza-bicyclo[2.2.1]hepten-(2). Justus Liebigs Ann. Chem. 1967, 702, 1–7.
- (19) Adam, W.; Grune, M.; Diedering, M.; Trofimov, A. V. Temperature and viscosity dependence in the stereoselective formation of the inverted housane for the photochemical nitrogen loss from the deuterium-stereolabeled parent diazabicyclo[2.2.1]hept-2-ene. J. Am. Chem. Soc. 2001, 123, 7109–7112.
- (20) Adam, W.; Diedering, M.; Trofimov, A. V. Solvent effects in the photodenitrogenation of the azoalkane diazabicyclo[2.2.1]hept-2-ene: viscosity- and polarity-controlled stereoselectivity in housane formation from the diazenyl diradical. *Phys. Chem. Chem. Phys.* **2002**, *4*, 1036–1039.
- (21) Adam, W.; Diedering, M.; Trofimov, A. V. Intriguing double-inversion stereochemistry in the denitrogenation of 2,3-diazabicyclo[2.2.1]heptene-type azoalkanes: a model mechanistic study in physical organic chemistry. *J. Phys. Org. Chem.* **2004**, *17*, 643–655.
- (22) Adam, W.; Denninger, U.; Finzel, R.; Kita, F.; Platsch, H.; Walter, H.; Zang, G. Comparative study of the pyrolysis, photo-induced electron transfer (PET), and laser-jet and 185-nm photo-

- chemistry of alkyl-substituted bicyclic azoalkanes. J. Am. Chem. Soc. 1992, 114, 5027–5035.
- (23) Yamamoto, N.; Olivucci, M.; Celani, P.; Bernardi, F.; Robb, M. A. An MC-SCF/MP2 Study of the Photochemistry of 2,3-Diazabicyclo[2.2.1]hept-2-ene: Production and Fate of Diazenyl and Hydrazonyl Biradicals. *J. Am. Chem. Soc.* **1998**, *120*, 2391–2407.
- (24) Sinicropi, A.; Page, C. S.; Adam, W.; Olivucci, M. Computational study on the origin of the stereoselectivity for the photochemical denitrogenation of diazabicycloheptene. *J. Am. Chem. Soc.* **2003**, *125*, 10947–10959.
- (25) Chen, H.; Li, S. CASPT2//CASSCF study on the photolysis mechanism of 2,3-diazabicyclo[2.1.1]hex-2-ene: alpha C-N versus beta C-C cleavage. *J. Org. Chem.* **2006**, *71*, 9013–9022.
- (26) Abe, M.; Hatano, S. Mechanistic study of stereoselectivity in azoalkane denitrogenations. *Pure Appl. Chem.* **2017**, *89*, 759–764.
- (27) Fdez Galvan, I.; Vacher, M.; Alavi, A.; Angeli, C.; Aquilante, F.; Autschbach, J.; Bao, J. J.; Bokarev, S. I.; Bogdanov, N. A.; Carlson, R. K.; Chibotaru, L. F.; Creutzberg, J.; Dattani, N.; Delcey, M. G.; Dong, S. S.; Dreuw, A.; Freitag, L.; Frutos, L. M.; Gagliardi, L.; Gendron, F.; Giussani, A.; Gonzalez, L.; Grell, G.; Guo, M.; Hoyer, C. E.; Johansson, M.; Keller, S.; Knecht, S.; Kovacevic, G.; Kallman, E.; Li Manni, G.; Lundberg, M.; Ma, Y.; Mai, S.; Malhado, J. P.; Malmqvist, P. A.; Marquetand, P.; Mewes, S. A.; Norell, J.; Olivucci, M.; Oppel, M.; Phung, Q. M.; Pierloot, K.; Plasser, F.; Reiher, M.; Sand, A. M.; Schapiro, I.; Sharma, P.; Stein, C. J.; Sorensen, L. K.; Truhlar, D. G.; Ugandi, M.; Ungur, L.; Valentini, A.; Vancoillie, S.; Veryazov, V.; Weser, O.; Wesolowski, T. A.; Widmark, P. O.; Wouters, S.; Zech, A.; Zobel, J. P.; Lindh, R. OpenMolcas: From Source Code to Insight. J. Chem. Theory Comput. 2019, 15, 5925–5964.
- (28) Jacquemin, D.; Perpète, E. A.; Ciofini, I.; Adamo, C. On the TD-DFT UV/vis spectra accuracy: the azoalkanes. *Theor. Chem. Acc.* **2008**, *120*, 405–410.
- (29) Pierloot, K.; Dumez, B.; Widmark, P.-O.; Roos, B. r. O. Density matrix averaged atomic natural orbital (ANO) basis sets for correlated molecular wave functions. *Theor. Chim. Acta* **1995**, *90*, 87–114.
- (30) Pou-Amérigo, R.; Merchán, M.; Nebot-Gil, I.; Widmark, P.-O.; Roos, B. O. Density matrix averaged atomic natural orbital (ANO) basis sets for correlated molecular wave functions. *Theor. Chim. Acta* 1995, 92, 149–181.
- (31) Widmark, P.-O.; Malmqvist, P.-K.; Roos, B. R. O. Density matrix averaged atomic natural orbital (ANO) basis sets for correlated molecular wave functions. *Theor. Chim. Acta* **1990**, *77*, 291–306.
- (32) Widmark, P.-O.; Persson, B. J.; Roos, B. O. Density matrix averaged atomic natural orbital (ANO) basis sets for correlated molecular wave functions. *Theor. Chim. Acta* **1991**, *79*, 419–432.
- (33) Roos, B. O.; Andersson, K. Multiconfigurational perturbation theory with level shift the Cr2 potential revisited. *Chem. Phys. Lett.* **1995**, 245, 215–223.
- (34) Roos, B. O.; Andersson, K.; Fülscher, M. P.; Serrano-Andrés, L.; Pierloot, K.; Merchán, M.; Molina, V. Applications of level shift corrected perturbation theory in electronic spectroscopy. *J. Mol. Struct.: Theochem.* **1996**, 388, 257–276.
- (35) Martyna, G. J.; Tuckerman, M. E.; Tobias, D. J.; Klein, M. L. Explicit reversible integrators for extended systems dynamics. *Mol. Phys.* **1996**, *87*, 1117–1157.
- (36) Hammes-Schiffer, S.; Tully, J. C. Proton transfer in solution: Molecular dynamics with quantum transitions. *J. Chem. Phys.* **1994**, 101, 4657–4667.
- (37) Tully, J. C. Molecular dynamics with electronic transitions. *J. Chem. Phys.* **1990**, 93, 1061–1071.
- (38) Tully, J. C.; Preston, R. K. Trajectory Surface Hopping Approach to Nonadiabatic Molecular Collisions: The Reaction of H+ with D2. *J. Chem. Phys.* **1971**, *55*, 562–572.
- (39) Reed, A. E.; Curtiss, L. A.; Weinhold, F. Intermolecular interactions from a natural bond orbital, donor-acceptor viewpoint. *Chem. Rev.* **1988**, *88*, 899–926.
- (40) Glendening, E. D.; Badenhoop, J. K.; Reed, A. E.; Carpenter, J. E.; Bohmann, J. A.; Morales, C. M.; Landis, C. R.; Weinhold, F. *NBO*

- 6.0, Theoretical Chemistry Institute, University of Wisconsin, Madison: 2013.
- (41) Perdew, J. P.; Burke, K.; Ernzerhof, M. Generalized Gradient Approximation Made Simple. *Phys. Rev. Lett.* **1996**, *77*, 3865–3868.
- (42) Perdew, J. P.; Burke, K.; Ernzerhof, M. Generalized Gradient Approximation Made Simple [Phys. Rev. Lett. 77, 3865 (1996)]. Phys. Rev. Lett. 1996, 77, 3865–3868.
- (43) Dunning, T. H. Gaussian basis sets for use in correlated molecular calculations. I. The atoms boron through neon and hydrogen. *J. Chem. Phys.* **1989**, *90*, 1007–1023.
- (44) Nesse, F. The ORCA program system. WIREs Comput. Mol. Sci. 2011, 2, 73–78.
- (45) Noodleman, L. Valence bond description of antiferromagnetic coupling in transition metal dimers. *J. Chem. Phys.* **1981**, *74*, 5737–5743.